



Research article

A reliable evaluation approach for multichannel signal denoising algorithms based on a novel arterial pulse acquisition system

Chao Chen^a, Zhendong Chen^a, Yuqi Zhou^b, Yinan Hao^c, Bo Peng^{c,d,*}, Xiaohua Xie^{a,**}, Haiqing Xie^e

^a School of Computer Science and Engineering, Sun Yat-Sen University, Guangzhou, 510006, China

^b Department of Pulmonary and Critical Care Medicine, The Third Affiliated Hospital of Sun Yat-sen University, Guangzhou 510630, China

^c Department of Musical Instrument Engineering, Xinghai Conservatory of Music, Guangzhou, 510006, China

^d Sniow Research and Development Laboratory, Foshan, 528000, China

^e School of Medical Engineering, Foshan University, Foshan 528000, China

ARTICLE INFO

Keywords:

Biomedical engineering
Pulse wave analysis
Multichannel pulse signals
Evaluation approach
Noise reduction
Denoising algorithms
Cardiovascular medicine

ABSTRACT

Background: Tactile sensors are utilized to measure multichannel pulse signals in pulse wave analysis (PWA). Owing to noise interferences, researchers have applied various denoising algorithms on multichannel pulse signals. To comprehensively assess these algorithms, numerous evaluation metrics have been proposed. However, these studies did not investigate the noise mechanisms in depth and lacked reference pulse signals, thus making the evaluations insufficiently objective.

Materials and methods: An applicable denoising evaluation approach for multichannel pulse signal algorithms based on an arterial pulse acquisition system is established by superimposing real-world multichannel noise to the reference signals. The system, comprising a SphygmoCor and a uniaxial noise acquisition device, allows us to acquire single-reference pulse signals as well as real-world multichannel noise.

Results: We assess eight popular denoising algorithms with three evaluation metrics, including amplitude relative error (ARE), mean square error (MSE) and increased percentage signal-noise ratio (SNR%). Our proposed approach provides accurate and objective evaluations of multichannel pulse signal denoising. Notably, classic algorithms for single-channel denoising are not recommended for multichannel denoising. Comparatively, RPCA-based algorithms can denoise pulse signals independently for each channel.

Conclusion: This study sets the stage for the establishment of accurate and objective pulse signal denoising evaluations and provides insights for data-driven clinical diagnoses in cardiovascular medicine.

1. Introduction

An important source of physiological information is the analysis of medical signals such as arterial pulse waves and electrocardiograms (ECG) [1–3]. Among these signals, the pulse waves are waves generated by cardiac ejection in heart cycles. Pulse wave

* Corresponding author. No.398 Outer Ring West Road, Guangzhou Higher Education Mega Center, Guangzhou, Guangdong, China.

** Corresponding author.

E-mail address: pengbo@xhcom.edu.cn (B. Peng).

<https://doi.org/10.1016/j.heliyon.2024.e26140>

Received 3 August 2023; Received in revised form 8 February 2024; Accepted 8 February 2024

Available online 20 February 2024

2405-8440/© 2024 Published by Elsevier Ltd.

This is an open access article under the CC BY-NC-ND license

(<http://creativecommons.org/licenses/by-nc-nd/4.0/>).

analysis (PWA) is regarded as a vital diagnostic tool in estimating cardiovascular disease (CVD) [4]. Some early pathological modifications like arterial stiffness and endothelial dysfunction can be estimated and diagnosed by cardiovascular parameters conducted from pulse wave analysis, such as heart rate, blood pressure, and pulse wave velocity [2,5–7]. In recent years, multichannel pulse signals have been measured widely with tactile sensors performed for physiological signals applications studies [8–11]. Multichannel arterial pulse signals are also called three-dimensional pulse images (3DPis), providing three-dimensional spatial and temporal characteristics of pulse waves [8].

Most 3DPis studies make use of the tactile sensors developed by PPS (Pressure Profile Systems Inc., Los Angeles, CA, USA), which are widely accepted as the preferred sensors for acquiring physiological signals in a wide range of clinical settings [12]. Noises of 3DPis include background noise, contact noise, and motion artefacts [13]. Intrinsic characteristics of multichannel sensor components cause the background noise of tactile sensors. While contacting the skin of participants, the physical properties of multichannel sensors are altered, resulting in contact noise. Furthermore, unconscious wrist movements and other physiological signals of participants may yield another type of noise called the motion artefacts. These three types of noises mainly compose the noise in 3DPis, which primarily influence the qualities of multichannel pulse signals and therefore lead to the inaccurate results of pulse wave analysis [14–17]. Additionally, the ECG is inherently sensitive and is consistently subject to corruption by power line and environmental noise interferences [18].

Some of these noises in pulse signals are difficult to eliminate since these noises are mixed with signals in the frequency domain. To reduce noise interference, researchers have performed various denoising methods for multichannel pulse signals. Some classic single-channel pulse signal denoising algorithms, such as Butterworth and wavelet, have been applied to multichannel pulse signal denoising in numerous studies [19–21]. Additionally, algorithms like Empirical Mode Decomposition (EMD) and Variational Mode Decomposition (VMD) are proposed for noise cancellation based on mode decomposition [22–25]. Another classic algorithm called Moving Average (MA) has also been applied in radial pulse signal denoising based on sliding windows [26]. However, these traditional algorithms cannot accommodate the denoising requirements for 3DPis because they perform the same denoising process for all channels. In recent years, in order to accommodate the denoising requirements for 3DPis, algorithms have been developed using Robust Principal Component Analysis based algorithms, including Robust Principal Component Analysis (RPCA), Weighted Principal Component Analysis (WRPCA), and Cross-Channel Dynamic Weighting Principal Component Analysis (cc-DWRPCA) [13,27,28].

The evaluation process of these denoising algorithms is vital since it can provide information regarding the performance in multichannel denoising. To assess these denoising algorithms comprehensively, numerous metrics are proposed. Wang et al. proposed a robust multichannel pulse signal pre-processing framework with a cascade filter based on frequency-dependent analysis (FDA). They also employed percentage mean error (PME), percentage standard deviation error (PSDE) and percentage smoothness (PS) to evaluate the processing results [26]. By evaluating these metrics, the quality of the filtered pulse signals can be quantitatively evaluated. Zou et al. treated the pulse signals measured by the intelligent pulse meter ZM-300 as the standard input pulse signals. They performed Dynamic Time Warping (DTW) distances, algorithm gains and magnitudes of changes in different test areas to compare the differences between standard input pulse signals and pulse signals with the processed processing method in the study [29]. They employed an objective device to capture the pulse signal, which conferred objectivity to the data. DTW can be applied to pulse signals since pulse signals are time-series signals. In the denoising study of Lu et al. [27], the multichannel pulse signals are modeled as the addition of original pulse signals, simulated static pressure and simulated noises. Mean-square error (MSE) and peak signal-to-noise ratio (PSNR), widely applied in numerous fields, including image and video processing, are employed to pulse signals in their study.

Nevertheless, detailed descriptions and demonstrations of these original pulse signals as reference signals are considerably limited, which remains a significant challenge in the current technology. Moreover, these simulated noises are captured by multichannel sensors without contacting the human body, which made these noises far different from noises in real-world environment. However, the current technologies denoise the pulse signals from the perspective of downstream tasks, which customarily neglects the requirements of reference pulse signals. The implementation of the reference signals can resolve these difficulties. With the reference pulse signals, evaluation metrics such as MSE and SNR are more convincing to perform in evaluations of denoising effects. With more convincing evaluation, medical staff and clinical investigators can identify optimal algorithms to denoise pulse signals. These filtered pulse signals can be employed to calculate more accurate physiological and clinical metrics, leading to reliable clinical diagnosis results [30].

Here, we propose a denoising evaluation approach for multichannel pulse signals based on arterial pulse signals from a novel system including a SphygmoCor (model EM3, AtCor Medical, Inc., Sydney, NSW, Australia) and a uniaxial noise acquisition device. This approach can yield clean multichannel reference pulse signals and real-world noises. In this system, we acquire a single channel signal from the SphygmoCor system, which is regarded as the recommended instrument with thousands of peer-reviewed literature in studies of physiological signal acquisition [31]. To simulate waveforms of other channels, channel attenuation factors (CAF) are produced according to the energy ratios of channels in a tactile sensor. Then, we establish a real-world measurement environment. In this study, we employ a uniaxial noise acquisition device to obtain noises of tactile sensors from all participants. The obtained noises contain the background noise, the contact noise and the motion artefacts. By adding the obtained noises into the reference signals, the signals for denoising are generated. We expand clean single channel pulse signals from the SphygmoCor into multiple-channel pulse signals by CAF. Simultaneously, we superimpose noise acquired from real-world measurements to generate reference signals. This process highlights the novelty of the system. Furthermore, we employ three objective evaluation metrics, non-deviation errors of key physiological points, mean square error (MSE) and increased percentage signal-noise-ratio (SNR%), to evaluate eight popular denoising algorithms (five classic algorithms: Butterworth, wavelet, EMD and VMD; and three RPCA-based methods: RPCA, WRPCA and cc-DWRPCA). Existing PPS tactile sensors to date are 12-channel sensors (3×4) and two 24-channel sensors ($4 \times 6, 5 \times 5-1$). A tactile array sensor can be constructed by arranging electrodes in orthogonal, overlapping strips. The electrodes overlap at each

point, forming a distinct capacitor. Capacitance and pressure are measured by selectively scanning a single row and column [32]. In this paper, a PPS sensor with 3 rows and 4 columns is marked as 3×4 . The $5 \times 5-1$ PPS sensor can provide a tactile centre point by placing the blank place in the corner [8]. These three generations of PPS tactile sensors are all used in the experiment to demonstrate the validity of our approach in sensors with different matrix forms. Overall, the approach in this study can support the clinical diagnoses with convincing evaluation of denoising algorithms and provides insights for other multichannel medical measurements.

The structure of the rest of this article is shown as follows. In the Materials and Methods section, the data acquisition method, the pre-processing methods, three evaluation metrics and de-noising methods for evaluation in our experiment are introduced. In the Results section, comparison of different de-noising methods and different PPS tactile sensors are presented. In the Discussion and Conclusion, we discuss the experimental results and draw the conclusions of this article.

2. Materials and Methods

A complete approach (Fig. 1) includes data acquisition, pre-processing, denoising algorithm implementation, and denoising algorithm evaluation (see Fig. 2).

A data acquisition system is used in the data acquisition module. The system includes a SphygmoCor device for acquiring single-reference pulse signals and a uniaxial noise acquisition device for acquiring real-world noises. SphygmoCor output signals and tactile sensor output signals are unified by custom mapping curves.

In the pre-processing module, a channel attenuation factor is calculated for each channel based on the energy ratios of the 12-channel pulse signal dataset [30]. With these CAFs, we can generate clean multi-reference pulse signals based on single-reference pulse signals. Reference pulse signals are converted according to the units of the output noise. Noise datasets of three generations of PPS tactile sensors are added in corresponding clean multi-reference pulse signals.

In the denoising algorithm implementation module, eight popular methods are applied, Butterworth, wavelet, VMD, EMD, MA, RPCA, WRPCA, and cc-DWRPCA. As RPCA-based algorithms denoise pulse signals by identifying the common features of different cycles in each channel, pulse signals from each channel are partitioned according to the cardiac cycles.

In the denoising algorithm evaluation module, evaluation metrics including non-deviation errors of key physiological points, MSE, and SNR are employed to evaluate the above eight denoising methods.

2.1. Data acquisition

This study utilizes a data acquisition system that includes both a SphygmoCor device and a uniaxial noise acquisition device. Single-reference pulse signals are recorded by the SphygmoCor device. Real-world noise is captured by the uniaxial noise acquisition device.

The SphygmoCor device is regarded as the recommended instrument with thousands of peer-reviewed literature in studies of physiological signal acquisition [31]. Through built-in operator index and noise reduction algorithms, the SphygmoCor device outputs a stable and clean signal at a sampling rate of 128 Hz [31], which is adopted as the single-reference pulse signal in this study.

Otherwise, we develop a uniaxial noise acquisition device, simplified from our uniaxial acquisition device, which provides repeatable radial artery data [7]. This uniaxial device includes a replaceable PPS sensor, a fixture, a robot finger, a stepper motor (used to adjust the depth of the robot finger pressing), and a main control board (Fig. 2). The sampling rates of the three generations of PPS

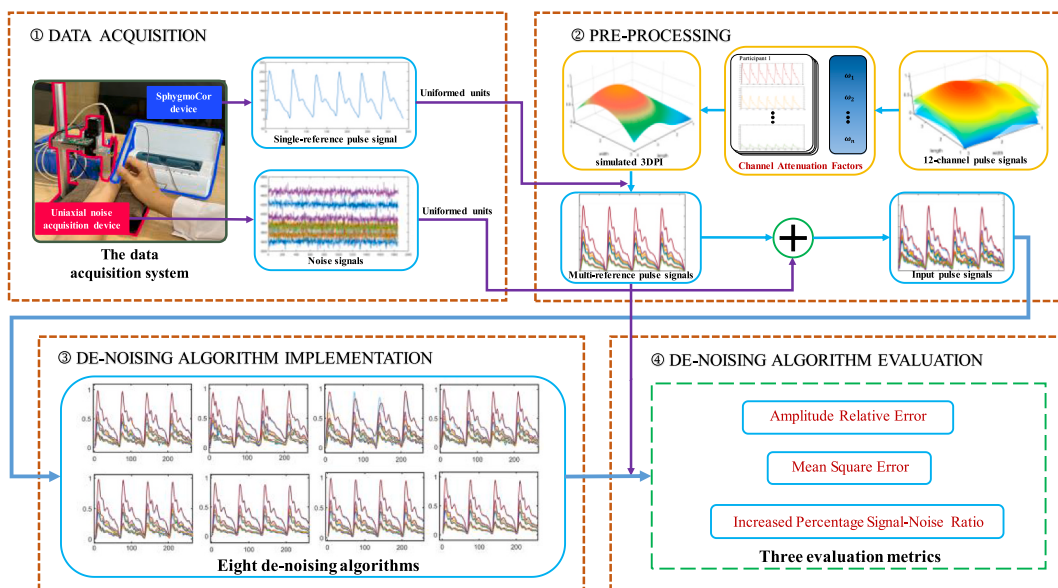


Fig. 1. Flow chart of the complete approach of denoising evaluation for multichannel arterial pulse signals.

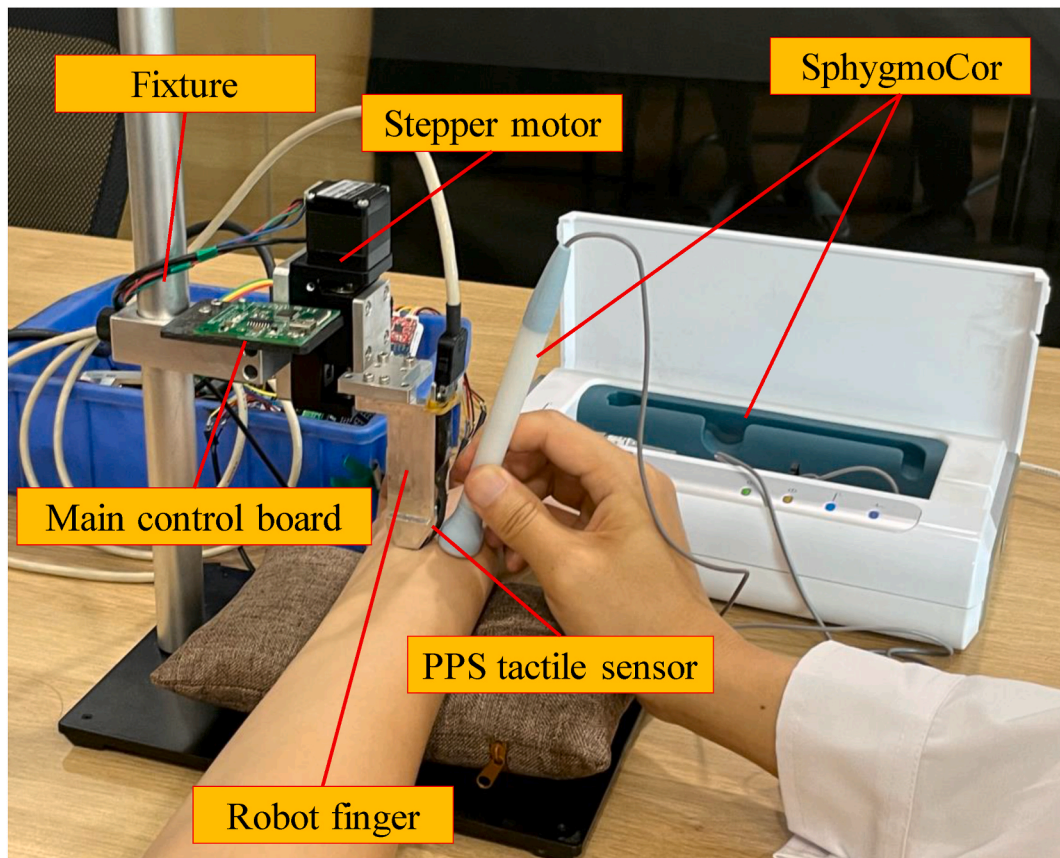


Fig. 2. The hardware composition of the data acquisition system (left: uniaxial noise acquisition device; right: SphygmoCor device [31]).

tactile sensors are unified to 85 Hz. The main control board (based on STM32 [33]) is responsible for controlling the underlying hardware, gathering PPS data, and communicating with the host computer via the serial port. The noise without pulse signals is measured using three generations of PPS tactile sensors, including a 12-channel PPS tactile sensor (3×4) and two 24-channel PPS tactile sensors (4×6 , $5 \times 5-1$). These three types of tactile sensors cover the most typical categories of available commercial PPS tactile sensors. To demonstrate the broad applicability of our approach, the tactile sensors in this study differ in terms of model, parameters, production years [8–10] and used times. Each experiment utilizes a specific PPS tactile sensor mounted on the robot finger and maintains a specific depth of the robot finger for a measurement pressure consistent with that of SphygmoCor close by the robot finger. Then, the noises on wrist surfaces next to radial arteries are captured by these tactile sensors, which are prominent 3DPI noises in real-world measurement environment but without pulse signals.

Besides, units for arterial pulse signals and tactile sensor output signals are unified using a mapping curve from the output value to pressure (mmHg).

Thirty noise time series and ten single-channel pulse signals are captured from five subjects, including one female and four males aged 27.60 ± 5.68 years (mean \pm SD). All subjects (systolic/diastolic blood pressure: $110.6 \pm 4.5/66.8 \pm 6.6$ mmHg) are randomly selected healthy students from Sun Yat-sen University. These two datasets are recorded under IRB approval (IRB#: [2020]-02-119-01).

2.2. Pre-processing

The single-channel and 12-channel pulse signals are employed to generate single-reference pulse signals. A Butterworth low-pass filter (first order low pass; zero-phase) with corner frequency

of 20 Hz is used to eliminate the high-frequency noise of the measured 12-channel pulse signals, and the baseline wandering is removed by a Butterworth low-pass filter (first order; zero-phase) with a cut-off frequency of 0.7 Hz [34,35]. The data cycle length of pulse signals by the tactile sensors (85 Hz) and SphygmoCor (128 Hz) are not equal due to the different sampling rates.

Channel attenuation factors (CAF) are calculated by comparing the signal energy of each sensor channel with the signal energy of the largest channel (the channel with the maximum signal energy). In addition, the absolute values of the factors are less than one. The CAF of each channel can be calculated as the following formula:

$$CAF_{n_c} = \frac{\sum_{n=1}^N a_{n_c,n}^2}{\sum_{n=1}^N a_{n_{max},n}^2} \quad (1)$$

where n_c is the number of the current channel, n indicates the current sample point, N denotes the total sampling points, $a_{n_c,t}$ and $a_{n_{max},t}$ are the amplitude of the pulse signals in the current channel and the largest channel.

With the CAF of each channel, the 3×4 , 4×6 and $5 \times 5-1$ reference pulse signals can be yielded.

This study uses the 12-channel pulse signal dataset to generate the CAFs, and in-depth descriptions of the dataset can be found in these papers [11,30]. The dataset consists of 24 healthy subjects at National Cheng Kung University (14 males and 10 females), each sampled at a rate of 100 Hz. CAFs are produced according to the energy ratios of channels in this dataset. Fig. 3(a) illustrates a superimposed stereoscopic 3DPI of the peak moments in the cardiac cycles of 24 subjects (see Fig. 4).

The single-reference pulse signals can be calculated as the following formula [37]:

$$D = S^T C \quad (2)$$

Where D denotes the matrix of the 12-channel reference pulse signals, S represents the single-channel pulse signal measured by the SphygmoCor System, and C is the CAF vector containing 12 CAFs adjusted by energy ratios of each channel in a 3×4 PPS tactile sensor.

The 12-channel reference pulse signals are reshaped into a 3×4 matrix according to the spatial arrangement of the 3×4 PPS tactile sensor. Then, a 60×60 matrix is derived from interpolation of the 3×4 matrix following the spatial arrangement of the PPS tactile sensor. Fig. 3(b) is the stereoscopic display of the simulated 3DPI (60×60 matrix) in this study. The 4×6 and $5 \times 5-1$ reference pulse signals are derived from the sampling of the 60×60 matrix following the spatial arrangement of the PPS tactile sensor, respectively.

A series of three reference pulse signals are resampled to match the noise sampling rate. Upon superimposing the noise over the reference pulse signals, the 3×4 , 4×6 and $5 \times 5-1$ input pulse signals are produced. The algorithm for generation of CAFs and reference pulse signal is described in Table 1.

2.3. Denoising algorithm implementation

Eight reliable denoising algorithms were performed in the experiments to verify our proposed evaluation approach. These algorithms are Butterworth, wavelet, VMD, EMD, MA, RPCA, WRPCA and cc-DWRPCA.

Butterworth filters are classic signal processing filters that provide a flat passband and do not impart any distortion to low-frequency components [19]. A Butterworth low pass filter (first order; zero-phase) with a cut-off frequency of 20 Hz is performed in this study. The wavelet filter provides temporal and spatial localization in the signals [38]. We perform a 4-level wavelet transform to decompose the input pulse signals and use the Birge-Massart algorithm to obtain the hard thresholds for the wavelet filter.

In this study, an EMD algorithm (sift relative tolerance: 0.2; sift max iterations: 100; maximum number of intrinsic mode function: 100; max extrema number: 1; max energy ratio: 20; interpolation: spline) is employed to denoise the input pulse signals. Besides, VMD methods (convergence criteria tolerance: $1e-7$; number of intrinsic mode function: 20; noise tolerance: 0; direct current component: 0; balancing parameter: 2000) are employed to denoising the input pulse signals. Another algorithm called MA is employed to identify the trend of the pulse signals to achieve noise cancellation. The window size of the MA filter is set to 3.

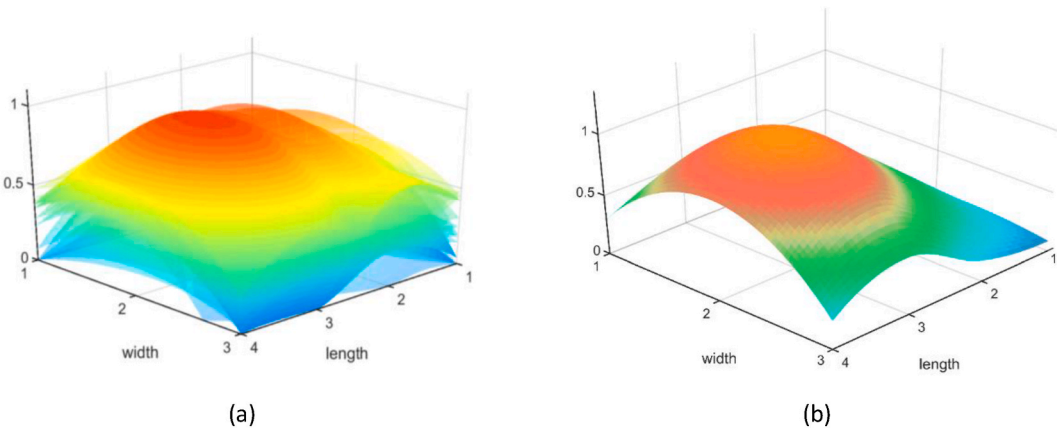


Fig. 3. Illustration of 3DPIs employed in this study. (a) the superimposed stereoscopic 3DPIs of 24 subjects (12-channel [8]); (b) the stereoscopic display of a simulated 3DPI (60×60 matrix). The x-axis and the y-axis of a 3D coordinate system define the pulse length along the direction of arterial blood flow while the pulse width corresponds to the pulse width perpendicular to that direction. The normalized z-axis represents the pulse amplitude measured with respect to 1 (violet is 0; red is 1).

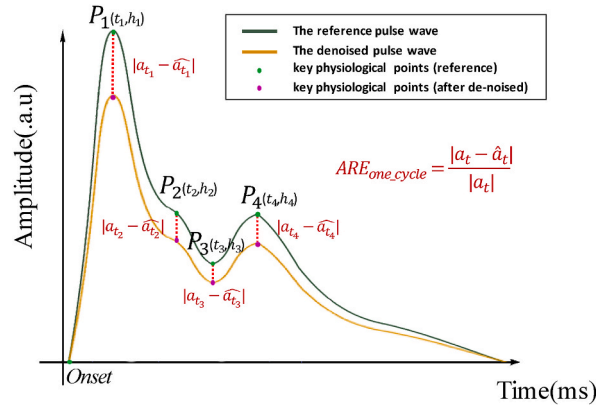


Fig. 4. Position of four key physiological points of the radial pulse wave and ARE calculation in a full cardiac cycle [36]: (a) Onset: aortic valve open; (b) P1: ventricular contraction; (c) P2: reflected wave; (d) P3: aortic valve closure; (e) P4: diastolic wave. t represents time, h represents the amplitude of each key physiological point, and a represents the amplitude of the single-reference pulse signals at each sampling point.

Table 1

Pseudo code for generation of CAFs and reference pulse signals.

Algorithm 1: Generation of CAFs and reference pulse signals

Input: Single-channel S and 12-channel pulse signals D

Output: CAF C and 3×4 , 4×6 and $5 \times 5-1$ reference pulse signals $D3 \times 4$, $D4 \times 6$ and $D5 \times 5-1$

1: Apply Butterworth filter to D

3: For each channel i in D

4: Calculate signal energy E_i

5: If $E_i > \max(\text{signal energy})$ $\max(E)$

6: $\max(E) = E_i$

7: $\max_channel = \text{current channel}$

8: Calculate C for each channel using formula (1)

9: For each channel in 12-channel pulse signals

10: Calculate single-reference pulse signals using formula (2)

11: Reshape D into $D3 \times 4$

12: Derive a 60×60 matrix $D60 \times 60$ from interpolation of the $D3 \times 4$

13: Sample $D4 \times 6$ and $D5 \times 5-1$ from $D60 \times 60$

RPCA-based methods. RPCA [27], Weighted RPCA [28] and cc-DWRPCA [13] are employed in this study. These algorithms denoise the pulse signals by extracting the common features of all cycles for every channel. The maximum iteration of RPCA-based methods is set to 1000. The convergence criteria tolerance is set to $1e-6$.

After performing the eight algorithms in the input pulse signals, the evaluation metrics are implemented to evaluate the denoising effects of these algorithms.

2.4. Denoising algorithm evaluation

Three types of metrics, including non-deviation errors of key physiological points, mean square error (MSE) and increased percentage signal-noise ratio (SNR%), are performed to evaluate the denoising methods in this study. A key contribution of our study is the generation of single-reference pulse signals. In this way, the process of comparing reference pulse signals with filtered pulse signals is accurate and reliable.

The amplitude relative error (ARE) is employed to measure the non-deviation error of key physiological points. Fig. 4 takes an example of a complete cardiac cycle [39]. Onset is created by the opening of the aortic valve. Then, the systolic wave rises to a peak (P_1). The second peak of the pulse wave (P_2) is caused by the backward wave from periphery branches. The diastolic notch (P_3) is linked to the closure of the arterial valve. The diastolic wave causes the third peak of the pulse wave (P_4). The amplitudes of these key physiological points are denoted as h_1 , h_2 , h_3 and h_4 . In many clinical scenarios, the peripheral augmented index (pAIx) is a vital estimation metric of vascular sclerosis is the ratio of the P_1 divided by the P_2 . Other related clinical metrics include h_3/h_1 and h_4/h_1 which can also reflect peripheral arterial resistance and stiffness [40–44]. In this study, we calculate the AREs of P_1 , P_2 , P_3 and P_4 before and after the denoising methods. Additionally, AREs of clinical metrics including pAIx, h_3/h_1 and h_4/h_1 are calculated to prove that our evaluation approach can facilitate clinical diagnoses.

The formula of ARE [13] is:

$$ARE = \frac{\sum_{n_p}^{N_p} \sum_{n_c}^{N_c} \frac{|a_i - \widehat{a}_i|}{|a_i|}}{N_p N_c} \tag{3}$$

Where N_p and N_c are the total number of cardiac cycles and channels, n_p and n_c are the number of the current cardiac cycle and channel, a_i is the amplitude of the single-reference pulse signals at each sampling point, and \widehat{a}_i is the amplitude of the filtered pulse signals at each sampling point.

The mean square error (MSE) is employed to compare the filtered pulse signals with the single-reference pulse signals. Since different channels in a PPS tactile sensor reflect additional spatial features of the pulse signals, data of all channels should be considered in the pulse signal denoising evaluation.

The average MSE of all channels in this study can be calculated as the following formula [42]:

$$MSE = \frac{\sum_{n_p}^{N_p} \sum_{n_c}^{N_c} (S_{n_p, n_c} - \widehat{S}_{n_p, n_c})^2}{N_c N_p} \tag{4}$$

Where S_p is the reference signal with the cardiac cycle p in the No. n_c channel, and \widehat{S}_{np} is the filtered signal with the cardiac cycle p in the No. n_c channel.

The increased percentage signal-to-noise ratio value (SNR%), derived from the signal-to-noise ratio (SNR), is used to determine the effectiveness of denoising methods in this study. The average SNR% of all channels is calculated to assess the performance of the denoising methods in the presence of interference [45,46]. The average SNR% can be calculated as the following formula:

$$SNR\% = \frac{SNR_{proc} - SNR_{ori}}{SNR_{proc}} \tag{5}$$

Where SNR_{proc} is the SNR after denoising, and SNR_{ori} is the SNR [46] before denoising. The SNR_{proc} and SNR_{ori} can be calculated as the following formulas:

$$SNR_{proc} = \frac{10 * \log_{10} \frac{\sum_{n_c=1}^{N_c} (S_{n_c})^2}{\sum_{n_c=1}^{N_c} (S_{n_c} - \widehat{S}_{n_c})^2}}{N_c} \tag{6}$$

$$SNR_{ori} = \frac{10 * \log_{10} \frac{\sum_{n_c=1}^{N_c} (S_{n_c})^2}{\sum_{n_c=1}^{N_c} (S_{n_c} - S_{n_c}')^2}}{N_c} \tag{7}$$

Where S_{n_c} is the reference signal in the No. n_c channel, S_{n_c}' is the input signal in the No. n_c channel, and \widehat{S}_{n_c} is the filtered signal in the No. n_c channel.

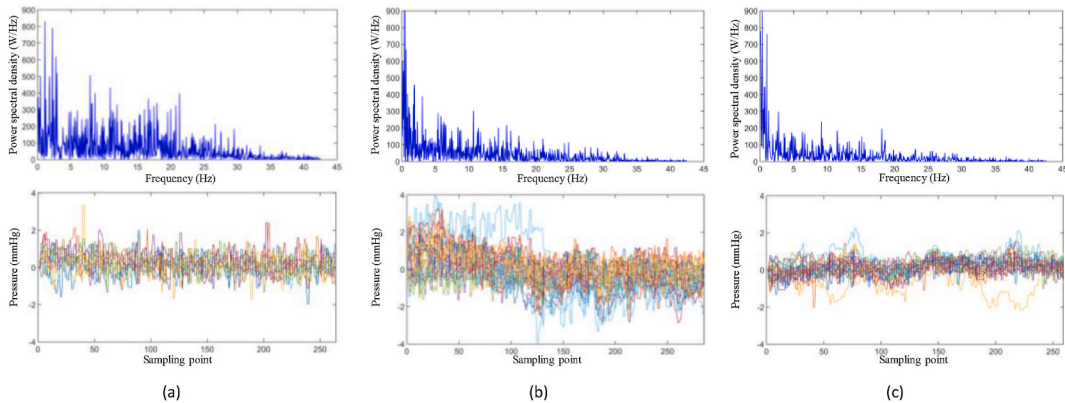


Fig. 5. Illustration of the waveforms and spectrums of the noise of some participants [13]. (a) the spectrum (upper) and the waveform (lower) of the noise in a 3 × 4 PPS tactile sensor; (b) the spectrum (upper) and the waveform (lower) of the noise in a 4 × 6 PPS tactile sensor; (c) the spectrum (upper) and the waveform (lower) of the noise in a 5 × 5–1 PPS tactile sensor.

3. Results

3.1. Data acquisition and pre-processing

Fig. 5 shows the time domain waveforms and spectra of the noise collected by three types of sensors. The noise data is incorporated into the 3×4 , 4×6 and $5 \times 5-1$ reference pulse signals (Fig. 6). The baseline wandering is removed by a Butterworth high-pass filter (first order low pass; zero-phase) with a cut-off frequency of 0.7 Hz. Finally, we obtain the input pulse signals (Fig. 7) (see Fig. 8) (see Fig. 6).

3.2. Denoising algorithm implementation

Fig. 8 illustrates the denoising effects of the 3×4 tactile sensors on a participant. Eight filtered pulse signals are present. All input pulse signals are normalized. The wavelet algorithm is particularly limited, but it is effective when dealing with small-amplitude channels. MA alters the time domain. EMD provides slightly better effects than wavelets. The Butterworth and VMD methods perform better, but the similarity of the cycles is weak. RPCA-based algorithms denoise well and have strong parallels to cardiac cycles. Among these three algorithms, the amplitudes after RPCA are too low, the performance of WRPCA is better in channels with large amplitudes compared to those with small amplitudes, and the performance of cc-DWRPCA is superior in all channels. These results suggest that cc-DWRPCA has better performances than other denoising algorithms. The following sections provide objective metrics and detailed analyses that will reinforce these conclusions.

3.3. Denoising algorithm evaluation

The channels with the greatest amplitudes of every subject are selected to assess the non-deviation errors of key physiological points before and after eight denoising algorithms. These channels contain several complete cardiac cycles.

In this study, we employ the amplitude relative errors (ARE) to evaluate the non-deviation errors of key physiological points [13]. The AREs calculated before and after denoising three types of tactile sensors are shown in Table 2. For the 3×4 tactile sensors, the cc-DWRPCA has the lowest ARE in the four key physiological points. For the 4×6 tactile sensors, the cc-DWRPCA exhibits the lowest ARE in P1, P2 and P4 while the RPCA has the lowest ARE in P3. For the $5 \times 5-1$ tactile sensors, the cc-DWRPCA has the lowest ARE in P3 and P4 while the Butterworth shows the lowest ARE in P1 and P2. On the whole, the MSEs for RPCA-based methods are 7.68% on average less than those for five classic algorithms. In addition, the MSEs for the cc-DWRPCA are 32.73% on average lower than those for the other seven algorithms.

The independent AREs in the results obey the normal distribution with homogeneous variance according to the k-s test, so we conduct a one-way ANOVA to compare AREs of all algorithms. The one-way ANOVA results in Table 2 indicate the significant difference among AREs of the eight algorithms. The following three tables also employ one-way ANOVA to indicate the significant difference.

Table 3 illustrates the AREs of pAIx, h3/h1 and h4/h1 calculated before and after denoising results of three types of tactile sensors. For all generations of tactile sensors, RPCA-based algorithms have the lowest ARE in the three clinical metrics compared with traditional algorithms. In these RPCA algorithms, cc-DWRPCA has the best performances in these metrics. Notably, for the $5 \times 5-1$ tactile sensors, Butterworth has the lowest ARE in pAIx.

Table 4 shows the MSEs for the three types of tactile sensors after eight denoising methods. The MSE results in Table 4 consider all channels of all participants. Table 4 shows that the cc-DWRPCA has the lowest MSE among eight algorithms in the 3×4 and $5 \times 5-1$ tactile sensors generally. The RPCA algorithm has the lowest MSE among eight algorithms in the 4×6 tactile sensors. Further, the MSE of the cc-DWRPCA also has the lowest MSE among these eight algorithms. Additionally, the 4×6 tactile sensors have larger MSEs than the other two types of tactile sensors. In general, the MSEs for RPCA-based methods are 45.4% on average less than those for the classic algorithms. Moreover, the MSEs for the cc-DWRPCA methods are 58% on average less than those for the other seven algorithms.

Table 5 shows the SNR% for three types of tactile sensors after eight denoising methods. The results in Table 4 represent the

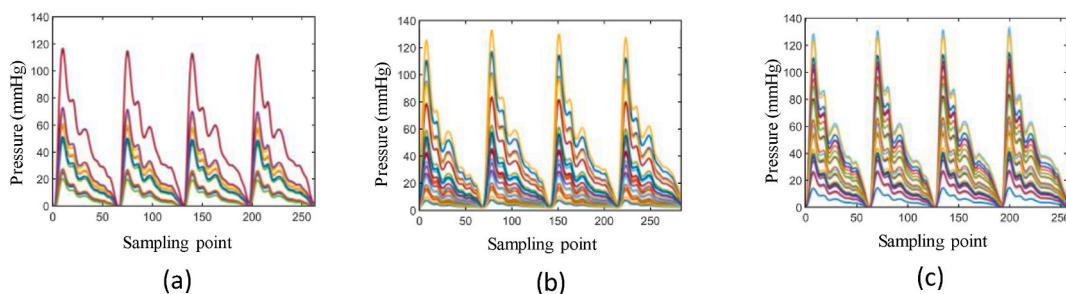


Fig. 6. Illustration of several typical reference pulse signals [13]. (a) reference pulse signals of a 3×4 PPS tactile sensor of a participant; (b) reference pulse signals of a 4×6 PPS tactile sensor of a participant; (c) reference pulse signals of a $5 \times 5-1$ PPS tactile sensor of a participant.

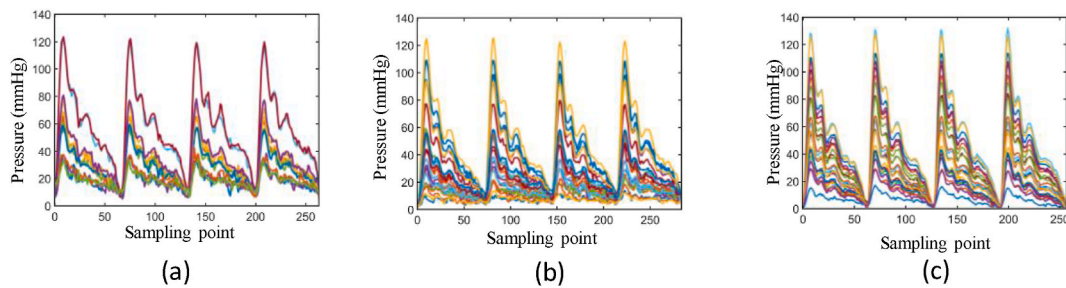


Fig. 7. Illustration of the input pulse signals with noise [13]: (a) input pulse signals of a 3×4 PPS tactile sensor of a participant; (b) input pulse signals of a 4×6 PPS tactile sensor of a participant; (c) input pulse signals of a $5 \times 5-1$ PPS tactile sensor of a participant.

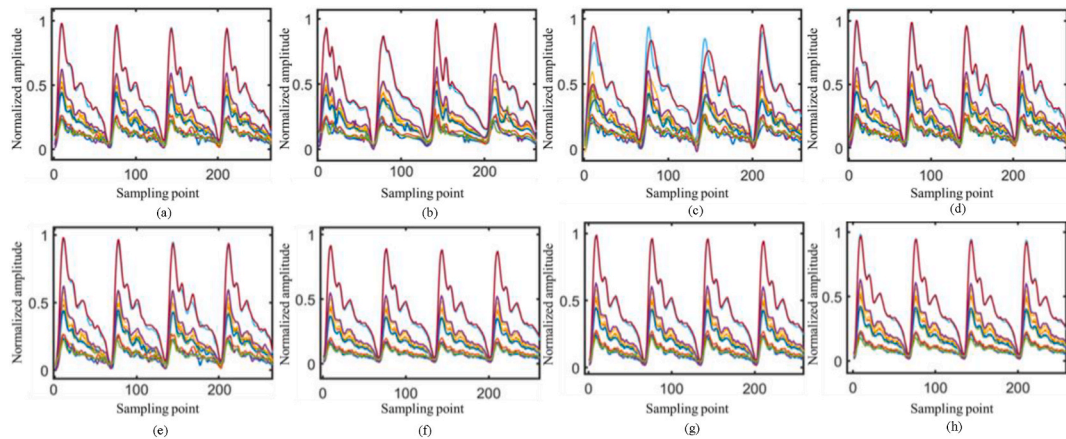


Fig. 8. Illustration of denoising effects of the 3×4 tactile sensors of a subject. (a). Butterworth [19]; (b). wavelet [20]; (c). Empirical Mode Decomposition (EMD) [22]; (d). Variational Mode Decomposition (VMD) [24]; (e). Moving Average (MA) [26]; (f). Robust Principal Component Analysis (RPCA) [27]; (g). Weighted Principal Component Analysis (WRPCA) [28]; (h). Cross-Channel Dynamic Weighting Principal Component Analysis (cc-DWRPCA) [13]. All input pulse signals are normalized.

average SNR% for all participants across all channels. **Table 5** shows that the cc-DWRPCA has the greatest SNR across three types of tactile sensors among eight algorithms (4.75% greater than those for the other seven algorithms), which means that the cc-DWRPCA has the best performance in eliminating the noises in multichannel pulse signals. Additionally, the SNR% of RPCA-based methods are generally greater than other classic algorithms (20.89% on average larger than those for five classic algorithms). Of five classic algorithms, the Butterworth algorithm has the greatest SNR%.

4. Discussion

This paper proposes a technically feasible pathway towards achieving a reliable and constructive evaluation of denoising algorithms in multichannel arterial pulse signals to facilitate accurate clinical diagnoses. In this approach, we capture the single-channel pulse signals with a SphygmoCor system and perform channel attenuation factors (CAFs) to create clean multi-reference pulse signals. Then, we design a uniaxial noise acquisition device to obtain real-world noises using three generations of tactile sensors (3×4 , 4×6 and $5 \times 5-1$). Eight denoising algorithms, including Butterworth, wavelet, EMD, VMD, MA, RPCA, WRPCA and cc-DWRPCA, are evaluated for 3DPI noise cancellation effects with MSE, SNR and non-deviation error evaluation. Notably, in the non-deviation error evaluation, three additional clinical metrics reflecting peripheral arterial resistance and stiffness are utilized to illustrate the clinical applicability of the approach.

In the results section, RPCA-based methods can extract specific features from multiple cycles in each single channel, which is theoretically suitable for multichannel pulse signal denoising. Compared with five classic algorithms (Butterworth, wavelet, EMD, VMD and MA), RPCA-based algorithms offer improved denoising performances in all three generations of tactile sensors in general. For example, in **Table 4**, the MSEs for RPCA-based methods are averagely 45.4% smaller than that for the classic algorithms. Experimental results, as well as previous knowledge, suggest that RPCA-based methods offer better noise removal performance.

Compared with RPCA and WRPCA, cc-DWRPCA employed channel scaled factors (CAFs) to adjust the weights in the nuclear norms in accordance with the signal pattern of each channel, which can adapt to the unique features of each channel. Comparatively to RPCA and WRPCA, cc-DWRPCA provides the most satisfactory denoising performances and superior ability to maintain cycle stability across all three generations of tactile sensors. For example, in **Table 5**, the SNRs for cc-DWRPCA are 4.75% on average larger than that for the

Table 2
AREs for four key physiological points of three types of tactile sensors after eight denoising methods.

		Butterworth [19]	Wavelet [20]	EMD [22]	VMD [24]	MA [26]	RPCA [27]	WRPCA [28]	cc-DWRPCA [13]	ANOVA ^a
3 × 4	P ₁	0.068 ± 0.029	0.093 ± 0.024	0.100 ± 0.030	0.071 ± 0.032	0.068 ± 0.024	0.197 ± 0.016	0.067 ± 0.033	0.062 ± 0.014	<i>p</i> < 0.05
	P ₂	0.141 ± 0.062	0.198 ± 0.066	0.154 ± 0.065	0.145 ± 0.065	0.170 ± 0.078	0.174 ± 0.024	0.143 ± 0.067	0.076 ± 0.020	<i>p</i> < 0.05
	P ₃	0.249 ± 0.134	0.378 ± 0.125	0.276 ± 0.141	0.249 ± 0.137	0.259 ± 0.132	0.166 ± 0.035	0.253 ± 0.147	0.139 ± 0.078	<i>p</i> < 0.05
	P ₄	0.168 ± 0.081	0.187 ± 0.083	0.172 ± 0.080	0.176 ± 0.085	0.159 ± 0.081	0.154 ± 0.018	0.143 ± 0.077	0.063 ± 0.034	<i>p</i> < 0.05
4 × 6	P ₁	0.239 ± 0.216	0.244 ± 0.202	0.270 ± 0.199	0.243 ± 0.215	0.230 ± 0.196	0.279 ± 0.084	0.258 ± 0.242	0.174 ± 0.144	<i>p</i> < 0.05
	P ₂	0.526 ± 0.323	0.583 ± 0.304	0.527 ± 0.322	0.529 ± 0.320	0.573 ± 0.347	0.307 ± 0.195	0.560 ± 0.392	0.258 ± 0.322	<i>p</i> < 0.05
	P ₃	0.934 ± 0.514	1.096 ± 0.507	0.939 ± 0.512	0.923 ± 0.512	0.952 ± 0.510	0.425 ± 0.331	0.939 ± 0.501	0.457 ± 0.410	<i>p</i> < 0.05
	P ₄	0.653 ± 0.429	0.645 ± 0.440	0.651 ± 0.422	0.662 ± 0.425	0.631 ± 0.426	0.325 ± 0.220	0.596 ± 0.362	0.258 ± 0.270	<i>p</i> < 0.05
5 × 5-1	P ₁	0.030 ± 0.023	0.077 ± 0.019	0.174 ± 0.068	0.078 ± 0.136	0.041 ± 0.019	0.246 ± 0.030	0.039 ± 0.025	0.038 ± 0.016	<i>p</i> < 0.05
	P ₂	0.060 ± 0.031	0.156 ± 0.043	0.124 ± 0.054	0.128 ± 0.214	0.077 ± 0.047	0.249 ± 0.037	0.087 ± 0.036	0.065 ± 0.012	<i>p</i> < 0.05
	P ₃	0.095 ± 0.057	0.258 ± 0.075	0.224 ± 0.129	0.222 ± 0.357	0.103 ± 0.064	0.224 ± 0.047	0.109 ± 0.064	0.074 ± 0.041	<i>p</i> < 0.05
	P ₄	0.074 ± 0.045	0.142 ± 0.039	0.096 ± 0.046	0.189 ± 0.307	0.070 ± 0.039	0.238 ± 0.035	0.063 ± 0.041	0.044 ± 0.019	<i>p</i> < 0.05

^a The one-way ANOVA results indicate the significant difference among AREs of the eight algorithms.

Table 3

AREs for three clinical metrics of three types of tactile sensors after eight denoising methods.

		Butterworth [19]	Wavelet [20]	EMD [22]	VMD [24]	MA [26]	RPCA [27]	WRPCA [28]	cc-DWRPCA [13]	ANOVA ^a
3 × 4	pAIx	0.095 ± 0.039	0.210 ± 0.067	0.152 ± 0.061	0.096 ± 0.038	0.138 ± 0.058	0.083 ± 0.032	0.084 ± 0.031	0.083 ± 0.031	<i>p</i> < 0.05
	h ₃ /h ₁	0.197 ± 0.094	0.419 ± 0.108	0.284 ± 0.106	0.187 ± 0.093	0.230 ± 0.096	0.178 ± 0.098	0.178 ± 0.095	0.177 ± 0.093	<i>p</i> < 0.05
	h ₄ /h ₁	0.116 ± 0.043	0.167 ± 0.062	0.169 ± 0.056	0.115 ± 0.043	0.122 ± 0.049	0.093 ± 0.038	0.093 ± 0.038	0.093 ± 0.038	<i>p</i> < 0.05
4 × 6	pAIx	0.225 ± 0.084	0.341 ± 0.115	0.262 ± 0.074	0.224 ± 0.084	0.280 ± 0.102	0.199 ± 0.069	0.197 ± 0.068	0.199 ± 0.069	<i>p</i> < 0.05
	h ₃ /h ₁	0.496 ± 0.158	0.762 ± 0.189	0.554 ± 0.139	0.477 ± 0.158	0.541 ± 0.160	0.451 ± 0.158	0.448 ± 0.157	0.448 ± 0.157	<i>p</i> < 0.05
	h ₄ /h ₁	0.324 ± 0.169	0.366 ± 0.175	0.374 ± 0.160	0.319 ± 0.165	0.331 ± 0.164	0.254 ± 0.101	0.248 ± 0.104	0.247 ± 0.105	<i>p</i> < 0.05
5 × 5-1	pAIx	0.045 ± 0.019	0.181 ± 0.069	0.292 ± 0.163	0.062 ± 0.037	0.089 ± 0.035	0.057 ± 0.018	0.056 ± 0.016	0.057 ± 0.019	<i>p</i> < 0.05
	h ₃ /h ₁	0.089 ± 0.039	0.341 ± 0.072	0.476 ± 0.258	0.131 ± 0.119	0.120 ± 0.048	0.084 ± 0.045	0.084 ± 0.043	0.083 ± 0.042	<i>p</i> < 0.05
	h ₄ /h ₁	0.064 ± 0.027	0.138 ± 0.045	0.242 ± 0.086	0.101 ± 0.096	0.071 ± 0.027	0.046 ± 0.019	0.045 ± 0.018	0.045 ± 0.017	<i>p</i> < 0.05

^a The one-way ANOVA results indicate the significant difference among AREs of the eight algorithms.

Table 4

MSEs for three types of tactile sensors after eight denoising methods.

	Butterworth [19]	Wavelet [20]	EMD [22]	VMD [24]	MA [26]	RPCA [27]	WRPCA [28]	cc-DWRPCA [13]	ANOVA ^a
3 × 4	0.006 ± 0.005	0.014 ± 0.010	0.011 ± 0.009	0.006 ± 0.005	0.010 ± 0.007	0.007 ± 0.004	0.005 ± 0.004	0.003 ± 0.003	$p < 0.05$
4 × 6	0.038 ± 0.073	0.049 ± 0.074	0.044 ± 0.072	0.039 ± 0.073	0.044 ± 0.073	0.019 ± 0.027	0.030 ± 0.053	0.020 ± 0.042	$p < 0.05$
5 × 5-1	0.003 ± 0.005	0.020 ± 0.016	0.037 ± 0.035	0.032 ± 0.096	0.011 ± 0.008	0.015 ± 0.010	0.004 ± 0.003	0.003 ± 0.002	$p < 0.05$

^a The one-way ANOVA results indicate the significant difference among MSEs of the eight algorithms.

Table 5
SNR% for three types of tactile sensors after eight denoising methods.

	Butterworth [19]	Wavelet [20]	EMD [22]	VMD [24]	MA [26]	RPCA [27]	WRPCA [28]	cc-DWRPCA [13]	ANOVA ^a
3 × 4	15.33 ± 6.022	11.58 ± 3.638	13.47 ± 5.142	15.15 ± 6.050	12.80 ± 4.309	14.47 ± 3.063	16.91 ± 6.454	19.32 ± 4.531	$p < 0.05$
4 × 6	10.98 ± 10.57	8.271 ± 8.288	9.555 ± 9.351	10.87 ± 10.55	9.092 ± 8.951	12.69 ± 6.892	11.98 ± 11.16	16.30 ± 8.933	$p < 0.05$
5 × 5-1	25.08 ± 5.373	16.75 ± 2.656	16.40 ± 4.616	20.10 ± 7.605	19.05 ± 3.104	15.61 ± 4.593	25.82 ± 5.188	27.28 ± 3.493	$p < 0.05$

^a The one-way ANOVA results indicate the significant difference among SNR% of the eight algorithms.

other seven algorithms. Theoretical and practical results demonstrate that cc-DWRPCA has superior noise cancellation capabilities.

Notably, Butterworth performs well in parts of our results and even outperforms some other algorithms in some evaluation metrics (see Table 2, 4 and 5). As a classic filter, the Butterworth provides outstanding denoising performances in pulse signals with the appropriate cut-off frequencies. However, Butterworth does not consider the common features of different cycles, making the waveforms of the denoised pulse signals more similar to the waveforms of the reference pulse signals. On the contrary, RPCA-based methods can extract the common features of different cycles in a channel, making the cycle variabilities closer to real-world pulse signals. Some examples of the results can serve as evidence. Because of the low cycle stability of the pulse samples, the Butterworth generally performs smaller AREs than the RPCA and WRPCA in the $5 \times 5 - 1$ group of AREs (Table 2). The stable cycle variability of the 3DPI samples in the 3×4 and 4×6 groups of MSEs (Table 4) results in RPCA-based algorithms having better MSE performances than five classic algorithms in general.

In this approach, certain clinical metrics that reflect vascular stiffness and elasticity are utilized to evaluate the efficacy of denoising algorithms. In Table 3, RPCA-based algorithms show the advantage across three types of tactile sensors among eight algorithms in $pAlx$, h_3/h_1 and h_4/h_1 . By obtaining superior denoising algorithms, medical staff and clinical investigators can make accurate assessments of pertinent clinical metrics [41]. These assessment outcomes directly affect diagnoses for cardiovascular disease [43]. Concurrently, the appropriate utilization of these metrics facilitates early disease diagnosis and management for patients, also empowering these patients to actualize more intuitive and reliable prognostic surveillances [42,44].

To our knowledge, this study provides some comprehensive and trustworthy evaluation metrics and assesses some famous denoising algorithms to date. At least three strengths make our proposed approach considerable utility in denoising evaluation.

The first strength is that we generate several clean multichannel pulse signals to be the reference pulse signals. This study expands the single-reference pulse signals to multi-reference pulse signals using CAFs. Since the amplitudes of different channels are determined by the energy of the current channels, these CAFs are generated according to the energy ratios of different channels [13]. This method can retain the complete information of the single-reference pulse signals and simulate real-world and objective nature of radial artery pulsation.

The second strength is that the noise data is derived from an objective source. In this study, we employ a uniaxial noise acquisition device to obtain the noise data from real-world environment. With the clean multi-reference pulse signals and real-world 3DPI noise, we retain the basic features of real-world pulse signals.

The third strength is that several objective and widely accepted evaluation metrics and clinical metrics are applied to evaluate the denoising performances of eight algorithms. MSE and SNR provide the similarity assessment between the reference pulse signals and the denoised pulse signals. Moreover, the application of non-deviation errors of key physiological points renders our approach more clinically relevant and meaningful.

This study indicates some promising directions for multichannel pulse signals denoising evaluation. These directions include evaluating denoising algorithms with clinical metrics and considering characteristics in different channels.

A shortcoming of the evaluation approach for multichannel signal denoising algorithms should be reported. The shortcoming lies in the sample size of the signal acquisition. In this study, we recruit five subjects to capture noise time series and single-channel pulse signals, which may be limited. Increasing the sample size can contribute to a more comprehensive and robust depiction of the multichannel pulse signals.

In terms of the prospects for the future, several enhancements may be envisaged for application in subsequent research. For instance, in future studies, tactile sensors with different technologies like PVDF, capacitive and piezoresistive can be considered [8,47]. It is vital to adapt and extend to different types of tactile sensors in order to improve the applicability of our approach. Another improvement is that the noise components can be extracted and analyzed. Some of these components, like respiratory signals and EMG signals, have been widely studied. A considerable amount of related research may be incorporated into our future studies. Additionally, a more sophisticated reference signal generation algorithm based on more samples that caters to distinctions between different channels in the real world may contribute to a more accurate and comprehensive evaluation. Overall, this approach has promising prospects in clinical diagnoses.

5. Conclusion

In this study, we propose a reliable and constructive approach for evaluating pulse signal denoising methods. Compared with other works, the main contribution of our approach is three-fold. First, we acquire a single-channel signal from the SphygmoCor system and use a CAF technique to simulate and yield the clean multi-reference pulse signals, making the evaluation solid, objective and convincing. Second, we collect the noise using our uniaxial noise acquisition device with standard multichannel sensors in real-world noise measurement environment. The proposed approach, superimposing real-world multichannel noise to a single-reference pulse signal, is particularly operational and applicable for the quantitative assessment of the denoising algorithm for multichannel pulse signals. Third, the denoising performances of eight popular algorithms are assessed using a variety of objective and widely accepted evaluation metrics. The experimental results indicate that the classic algorithms for single-channel denoising are not the recommended solution for 3DPI denoising. Comparatively to classic algorithms, RPCA-based algorithms are capable of denoising 3DPIs by extracting features from each channel independently. RPCA-based algorithms offer improved denoising performances in all three generations of tactile sensors in general. Especially, cc-DWRPCA has the most improved denoising performance. These experiments validate the theoretical hypothesis and prove the accuracy and objectivity of the denoising evaluation approach for multichannel arterial pulse signals. Our proposal provides the basis for the establishment of objective measurement frameworks and harbors great potentials to enable optimized signal processing and data-driven clinical diagnoses in cardiovascular medicine and beyond.

Financial support

This work was partially funded by National Natural Science Foundation of China, grant number 62071497.

Ethical statement

All procedures performed in studies involving human participants were approved by the Institutional Review Board of Sun Yat-sen University (approval#[2020]02-119-01). This study was conducted in accordance with the Declaration of Helsinki.

Data availability statement

The data generated and analyzed for this study are available from the corresponding author upon reasonable request. Due to the contractual agreement with the participants, if there is a need for these data, they can be obtained by contacting the corresponding author.

CRediT authorship contribution statement

Chao Chen: Writing – review & editing, Writing – original draft, Methodology. **Zhendong Chen:** Writing – review & editing, Validation, Methodology. **Yuqi Zhou:** Data curation. **Yinan Hao:** Validation. **Bo Peng:** Writing – review & editing, Supervision, Data curation. **Xiaohua Xie:** Supervision. **Haiqing Xie:** Data curation.

Declaration of competing interest

The authors declare that they have no known competing financial interests or personal relationships that could have appeared to influence the work reported in this paper.

Acknowledgements

The authors are grateful to Dr. Xinxin Li for her time and effort in critically reviewing this paper and providing constructive suggestions for improvement.

References

- [1] A. Kalra, A. Lowe, A. Al-Jumaily, Critical review of electrocardiography measurement systems and technology, *Meas. Sci. Technol.* 30 (1) (2019), <https://doi.org/10.1088/1361-6501/aaf2b7>.
- [2] M. AlGhatrif, J. Strait, C. Morrell, M. Canepa, J. Wright, P. Elango, et al., Longitudinal trajectories of arterial stiffness and the role of blood pressure: the Baltimore longitudinal study of aging, *Hypertension* 62 (5) (2013) 934–941, <https://doi.org/10.1161/HYPERTENSIONAHA.113.01445>.
- [3] N. Xiong, W. Liu, J. Li, S. Luo, W. Gu, W. Zhu, et al., Subclinical cardiac involvement present as electrocardiographic abnormalities in various neuromuscular diseases, *Heliyon* 9 (3) (2023) e13940, <https://doi.org/10.1016/j.heliyon.2023.e13940>.
- [4] G. Chen, C. Au, J. Chen, Textile triboelectric nanogenerators for wearable pulse wave monitoring, *Trends Biotechnol.* 39 (10) (2021) 1078–1092, <https://doi.org/10.1016/j.tibtech.2020.12.011>.
- [5] Y. Matsuzawa, T. Kwon, R. Lennon, L. Lerman, A. Lerman, Prognostic value of flow-mediated vasodilation in brachial artery and fingertip artery for cardiovascular events: a systematic review and meta-analysis, *J. Am. Heart Assoc.* 4 (11) (2015) 959–960, <https://doi.org/10.1161/JAHA.115.002270>.
- [6] S. Francque, D. Van Der Graaff, W. Kwanten, Non-alcoholic fatty liver disease and cardiovascular risk: pathophysiological mechanisms and implications, *J. Hepatol.* 65 (2) (2016) 425–443, <https://doi.org/10.1016/j.jhep.2016.04.005>.
- [7] T. Ohkuma, T. Ninomiya, H. Tomiyama, K. Kario, S. Hoshida, Y. Kita, et al., Brachial-ankle pulse wave velocity and the risk prediction of cardiovascular disease: an individual participant data meta-analysis, *Hypertension* 69 (6) (2017) 1045–1052, <https://doi.org/10.1161/HYPERTENSIONAHA.117.09097>.
- [8] B. Peng, C. Luo, W. Chan, M. Shieh, C. Su, C. Tai, Development and testing of a prototype for 3D radial pulse image measurement and compatible with 1D pulse wave analysis, *IEEE Access* 7 (2019) 182846–182859, <https://doi.org/10.1109/access.2019.2960338>.
- [9] Y. Chung, C. Hu, Y. Chu, C. Luo, X. Si, Exploring the conventional pulse conditions using Bi-sensing pulse diagnosis instrument, in: 4th International Conference on Biomedical Engineering and Informatics, IEEE, Shanghai, China, Shanghai, China, 2011, pp. 744–748, <https://doi.org/10.1109/BMEI.2011.6098473>.
- [10] K. Kong, W. Lau, B. Wong, H. Chan, B. Lee, B. Shen, et al., A pulse-sensing robotic hand for tactile arterial palpation, in: 2016 IEEE International Conference on Cyber Technology in Automation, Control, and Intelligent Systems, IEEE, Chengdu, China, 2016, pp. 141–145, <https://doi.org/10.1109/CYBER.2016.7574811>.
- [11] Z. Zhang, B. Peng, C.-H. Luo, C.-C. Tai, ANFIS-GA system for three-dimensional pulse image of normal and string-like pulse in Chinese medicine using an improved contour analysis method, *European Journal of Integrative Medicine* 42 (2021) 101301–101309, <https://doi.org/10.1016/j.eujim.2021.101301>.
- [12] J. Cui, L. Tu, J. Zhang, S. Zhang, Z. Zhang, J. Xu, Analysis of pulse signals based on array pulse volume, *Chin. J. Integr. Med.* 25 (2) (2019) 103–107, <https://doi.org/10.1007/s11655-018-2776-y>.
- [13] B. Peng, K.F. Gong, Z.D. Chen, C. Chen, Z. Zhang, X.H. Xie, et al., Cross-Channel dynamic weighting RPCA: a de-noising algorithm for multi-channel arterial pulse signal, *Appl Sci-Basel.* 12 (6) (2022) 2931, <https://doi.org/10.3390/app12062931>.
- [14] S. Pyo, J. Choi, J. Kim, Flexible, transparent, sensitive, and crosstalk-free capacitive tactile sensor array based on graphene electrodes and air dielectric, *Advanced Electronic Materials* 4 (1) (2018) 1700427, <https://doi.org/10.1002/aelm.201700427>.
- [15] M. Sohgawa, T. Uematsu, W. Mito, T. Kanashima, M. Okuyama, H. Noma, Crosstalk reduction of tactile sensor array with projected cylindrical elastomer over sensing element, *Jpn. J. Appl. Phys.* 50 (6) (2011), <https://doi.org/10.1143/jjap.50.06gm08>, 06GM8.
- [16] X. Xie, H. Liu, M. Shu, Q. Zhu, A. Huang, X. Kong, et al., A multi-stage denoising framework for ambulatory ECG signal based on domain knowledge and motion artifact detection, *Future Generat. Comput. Syst.* 116 (2021) 103–116, <https://doi.org/10.1016/j.future.2020.10.024>.
- [17] M. Singha Roy, R. Gupta, J.K. Chandra, K. Das Sharma, A. Talukdar, Improving photoplethysmographic measurements under motion artifacts using artificial neural network for personal healthcare, *IEEE Trans. Instrum. Meas.* 67 (12) (2018) 2820–2829, <https://doi.org/10.1109/tim.2018.2829488>.
- [18] P. Thamarai, Dr.K.Adalarasu, Denoising of EEG, ECG and PPG signals using wavelet transform, *J. Pharmaceut. Sci. Res.* 10 (1) (2018) 156–161, <https://doi.org/10.2139/ssrn.3356368>.

- [19] J. Roberts, D. Roberts T, Use of the Butterworth low-pass filter for oceanographic data, *J. Geophys. Res.* 83 (C11) (1978) 5510–5514, <https://doi.org/10.1029/JC083iC11p05510>.
- [20] J. Li, R. Li, Z. Chen, G. Deng, H. Wang, C. Mavromoustakis, et al., Design of a continuous blood pressure measurement system based on pulse wave and ECG signals, *IEEE Journal of Translational Engineering in Health and Medicine* 6 (2018) 1–14, <https://doi.org/10.1109/JTEHM.2017.2788885>.
- [21] O. Ken, K. Shouhei, I. Hiroaki, F. Seiya, F. Keisaku, Simultaneous measurement of heart sound, pulse wave and respiration with single fiber bragg grating sensor, in: 2018 IEEE International Symposium on Medical Measurements and Applications (MeMeA); 11–13 June 2018, IEEE, Rome, Italy, 2018, pp. 1–5, <https://doi.org/10.1109/MeMeA.2018.8438629>.
- [22] B. Huang, A. Kunoth, An optimization based empirical mode decomposition scheme, *J. Comput. Appl. Math.* 240 (2013) 174–183, <https://doi.org/10.1016/j.cam.2012.07.012>.
- [23] N. Huang, Z. Shen, S. Long, M. Wu, H. Shih, Q. Zheng, et al., The empirical mode decomposition and the hilbert spectrum for nonlinear and non-stationary time series analysis, in: *Proceedings of the Royal Society of London Series A: Mathematical, Physical and Engineering Sciences*, vol. 454, 1971, pp. 903–995, <https://doi.org/10.1098/rspa.1998.0193>, 1998.
- [24] Z. Wu, N. Huang, Ensemble empirical mode decomposition: a noise-assisted data analysis method, *Adv. Adapt. Data Anal.* 1 (1) (2011) 1–41, <https://doi.org/10.1142/s1793536909000047>.
- [25] P. Tavallali, T.Y. Hou, D.G. Rinderknecht, N.M. Pahlevan, On the convergence and accuracy of the cardiovascular intrinsic frequency method, *R. Soc. Open Sci.* 2 (12) (2015) 150475, <https://doi.org/10.1098/rsos.150475>.
- [26] D. Wang, D. Zhang, G. Lu, A robust signal preprocessing framework for wrist pulse analysis, *Biomed. Signal Process Control* 23 (2016) 62–75, <https://doi.org/10.1016/j.bspc.2015.08.002>.
- [27] J. Lu, X. Xie, B. Peng, C. Luo, Interference reduction by using RPCA and variational mode decomposition in 3D pulse images, in: *Proceedings of the 2019 4th International Conference on Multimedia Systems and Signal Processing*, Association for Computing Machinery, 2019, pp. 140–144, <https://doi.org/10.1145/3330393.3330397>.
- [28] L. He, C. Luo, X. Xie, B. Peng, De-noising of 3D pulse images by channel-weighted robust principal component analysis, in: 2019 IEEE 11th International Conference on Advanced Infocomm Technology 18–20 Oct. 2019, IEEE, 2019, pp. 19–23, <https://doi.org/10.1109/icaict.2019.8935929>.
- [29] H. Zou, Y. Zhang, J. Zhang, C. Chen, X. Geng, S. Zhang, et al., A novel multi-dimensional composition method based on time series similarity for array pulse wave signals detecting, *Algorithms* 13 (11) (2020) 297, <https://doi.org/10.3390/a13110297>.
- [30] B. Peng, C. Luo, N. Sinha, C. Tai, X. Xie, H. Xie, Fourier series analysis for novel spatiotemporal pulse waves: normal, taut, and slippery pulse images, *Evid. base Compl. Alternative Med.* 2019 (2019) 1–9, <https://doi.org/10.1155/2019/5734018>.
- [31] M. Butlin, A. Qasem, Large artery stiffness assessment using SphygmoCor technology, *Pulse (Basel)* 4 (4) (2017) 180–192, <https://doi.org/10.1159/000452448>.
- [32] C.S. Hu, Y.F. Chung, C.C. Yeh, C.H. Luo, Temporal and spatial properties of arterial pulsation measurement using pressure sensor array, *Evid Based Complement Alternat Med* 2012 (2012) 1–9, <https://doi.org/10.1155/2012/745127>.
- [33] C. Jin, C. Xia, S. Zhang, L. Wang, Y. Wang, H. Yan, A wearable combined wrist pulse measurement system using airbags for pressurization, *Sensors* 19 (2) (2019), <https://doi.org/10.3390/s19020386>.
- [34] J. Kozumplik, I. Provaznik, Fast time-varying linear filters for suppression of baseline drift in electrocardiographic signals, *Biomed. Eng. Online* 16 (1) (2017) 1–16, <https://doi.org/10.1186/s12938-017-0316-0>.
- [35] L. Sornmo, Time-varying digital filtering of ECG baseline wander, *Med. Biol. Eng. Comput.* 31 (5) (1993) 503–508, <https://doi.org/10.1007/BF02441986>.
- [36] Z. Chen, B. Peng, Y. Zhou, Y. Hao, X. Xie, Interpretable and accurate curve-fitting method for arterial pulse wave modeling and decomposition, *Int J Numer Method Biomed Eng* (2023) e3775, <https://doi.org/10.1002/cnm.3775>.
- [37] K. Hoffman, R. Kunze, *Linear Algebra*, Prentice Hall, America, 1971, <https://doi.org/10.2307/3617032>.
- [38] B. Goyal, A. Dogra, S. Agrawal, B. Sohi, A. Sharma, Image denoising review: from classical to state-of-the-art approaches, *Inf. Fusion* 55 (2020) 220–244, <https://doi.org/10.1016/j.inffus.2019.09.003>.
- [39] C. Su, T. Huang, C. Luo, Arterial pulse analysis of multiple dimension pulse mapping by local cold stimulation for arterial stiffness, *IEEE Sensor. J.* 16 (23) (2016) 8288–8294, <https://doi.org/10.1109/jsen.2016.2582805>.
- [40] L.J. Qiao, Z. Qi, L.P. Tu, Y.H. Zhang, L.P. Zhu, J.T. Xu, et al., The association of radial artery pulse wave variables with the pulse wave velocity and echocardiographic parameters in hypertension, *Evid Based Complement Alternat Med* 2018 (2018) 5291759, <https://doi.org/10.1155/2018/5291759>.
- [41] Y.N. Tsai, Y.H. Chang, Y.C. Huang, S. Jui-Shan Lin, S.M. Lee, Y.Y. Cheng, et al., The use of time-domain analysis on the choice of measurement location for pulse diagnosis research: a pilot study, *J. Chin. Med. Assoc.* 82 (1) (2019) 78–85, <https://doi.org/10.1016/j.jcma.2018.07.002>.
- [42] C.K. Zhang, L. Liu, W.J. Wu, Y.Q. Wang, H.X. Yan, R. Guo, et al., Identifying coronary artery lesions by feature analysis of radial pulse wave: a case-control study, *BioMed Res. Int.* 2021 (2021) 5047501, <https://doi.org/10.1155/2021/5047501>.
- [43] Z.J. Bi, X.H. Yao, X.J. Hu, P. Yuan, X.J. Guo, Z.L. Guo, et al., Assessment parameters for arrayed pulse wave analysis and application in hypertensive disorders, *Evid Based Complement Alternat Med* 2022 (2022) 6652028, <https://doi.org/10.1155/2022/6652028>.
- [44] W. Wang, W. Zeng, X. Chen, L. Tu, J. Xu, X. Yin, Parameter study on characteristic pulse diagram of polycystic ovary syndrome based on logistic regression analysis, *J. Obstet. Gynaecol.* 42 (8) (2022) 3712–3719, <https://doi.org/10.1080/01443615.2022.2158317>.
- [45] K.A. P T, Denoising of EEG, ECG and PPG signals using wavelet transform, *J. Pharmaceut. Sci. Res.* 10 (1) (2018) 156–161, <https://doi.org/10.2139/ssrn.3356368>.
- [46] Y. Xia, C. Chen, M. Shu, R. Liu, A denoising method of ECG signal based on variational autoencoder and masked convolution, *J. Electrocardiol.* 80 (2023) 81–90, <https://doi.org/10.1016/j.jelectrocard.2023.05.004>.
- [47] C. Chi, X. Sun, N. Xue, T. Li, C. Liu, Recent progress in technologies for tactile sensors, *Sensors* 18 (4) (2018) 948, <https://doi.org/10.3390/s18040948>.